BULLETIN OF THE EARTHQUAKE
RESEARCH INSTITUTE
UNIVERSITY OF TOKYO
Vol. 67 (1992), pp. 21–36

Volume Visualization of Seismicity

Tameshige TSUKUDA,[1] Katsumi MIURA,[1] Kimiaki FUJIWARA,[2]
Ken'etsu HANABUSA[3] and Teruo YAMASHITA[1]

[1] Earthquake Research Institute, University of Tokyo
[2] Institute of Computational Fluid Dynamics Co., Ltd.
[3] SIG (System Integrators Group) Co., Ltd.

(Received December 26, 1991)

Abstract

Spatial and temporal patterns of seismicity are visualized on color computer graphics by a method of semi-transparent volume rendering. Shading and classification procedures are applied to the influence function, the sum of the individual influence functions which are either Gaussian or quadratic in space and exponential in time in reference to the hypocenters and origin times of corresponding seismic events. Microearthquakes in a subducting plate were analyzed to show typical examples of 3-D images displaying outlines of seismic regions and indicating how the neighboring seismic activities are synchronized.

1. Introduction

Figures and diagrams on hypocentral parameters of earthquakes are indispensable to the studies on seismicity. The most common method is to plot epicenters on a two dimensional geographical map, with some symbols associated with their magnitudes, focal depths and/or observation periods. A primitive three-dimensional (3-D) image of hypocenters is realized by projecting their spots on the horizontal and two orthogonal vertical planes as shown in Fig. 1. Furthermore, pairs of pictures for stereographic views have been used for the study of 3-D configuration of hypocenters. Such figures merely show locations of independently distributed earthquake foci, and the complexity due to a considerable number of data points on a paper sheet makes it extremely difficult for us to extract characteristic distribution patterns. To clear this bottleneck, we prepare contour maps of number density of earthquakes (e.g., OIKE, 1976; TSUKUDA, 1990).

The method of contours in 2-D space can be extended to 3-D space. Isovalue surfaces for the density distributions are 3-D substitutes for 2-D contour lines. Now that techniques for scientific visualization in computer graphics (CG) are rapidly developing (THALMANN, 1990; PATRIKALAKIS, 1991), it is not too early to undertake seismic visualization to obtain 3-D silhouetted images of hypocentral distribution.

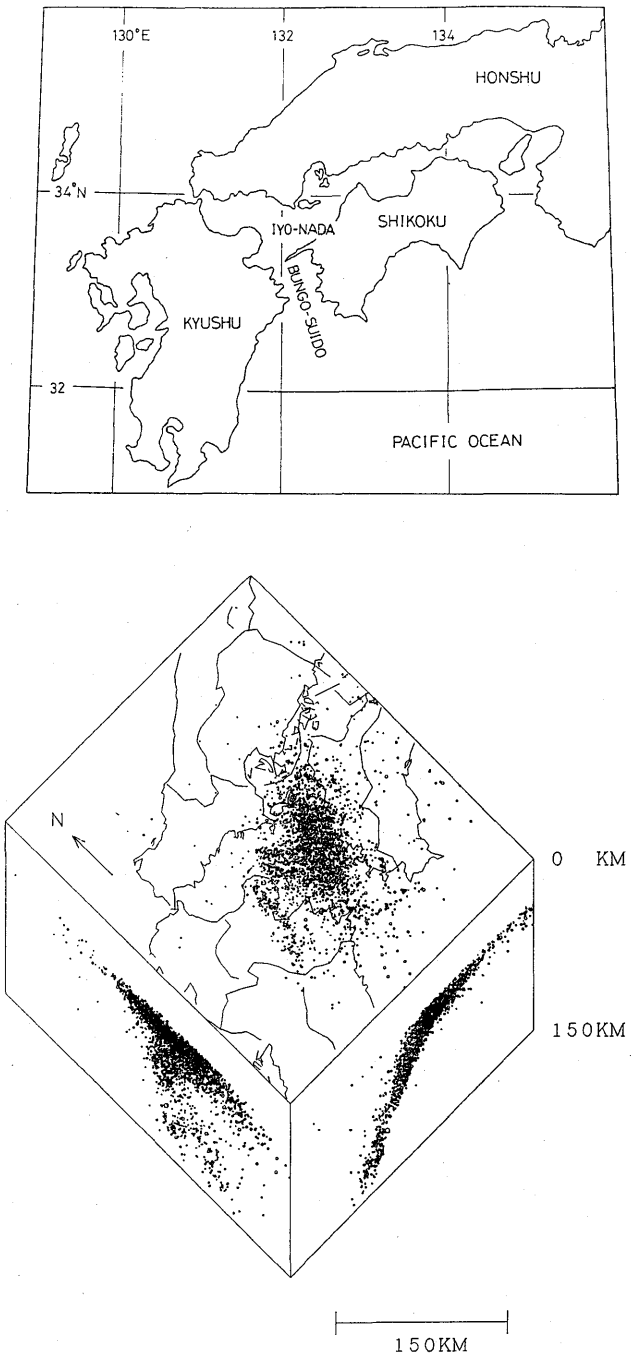

Fig. 1. 3-D distribution of intermediate depth microearthquakes ($M \geq 2$, 35 km $\leq$ focal depth $<$ 150 km) beneath the Iyo-Nada (the Sea of Iyo) and Bungo-Suido (the Bungo Channel) region between Shikoku and Kyushu Islands.
The observation period is from July 21, 1983 to December 31, 1990.

The second purpose of promoting the application of CG is to extend the space of the analysis into four-dimensions, i.e., space-time. Conventionally, space versus time diagrams are obtained by projecting on the two-dimensional space with reduced information. MOGI (1968) studied the migration of epicenters along some seismic active zones, making a diagram in which the distance measured from a certain point along the zone and the elapsed time are taken as ordinate and abscissa, respectively. KELLER (1970) used a similar space-time diagram by projecting the epicentral data on an axis in a certain direction. OIKE (1980) studied, utilizing a similar graph, the temporal change of distances between the focus of a moderate-sized earthquake and the surrounding foci of smaller events, and found that a seismicity gap is created before the earthquake. To study synchronized seismic activities along some seismic zones, MIZOUE *et al.* (1975) drew linkage lines between any two events close in space and time to each other. An accumulated set of those lines which forms a lineament pattern may indicate possible latent active faults within the crust. It sometimes is not easy to delineate lineaments from the complicated patterns of lines. One reason for this is an excess number of accumulated data points for a long time interval. Therefore, the seismic activities on the map should disappear after a certain elapsed time. TSUKUDA (1989a) put forward an idea of a time dependent seismicity map, where the radii of the epicentral circles tend to decrease with time.

This paper is along the line of the above studies and presents a new method for displaying four-dimensional seismicity on computer graphics. The technical point is how to visualize the continuum image of the spatial and temporal distribution for originally discontinuous point data. The essential part of the computation scheme is based on the paper by LEVOY (1988), who applied his so-called semi-transparent volume rendering to the data from computed tomography (CT). This general-purpose technique is effective even for displaying weak or fuzzy surfaces of a 3-D object, which may be precluded by other rendering methods to fit geometric primitives. A similar treatment for discrete points as ours was studied by NAGASAWA and KUWAHARA (1991) in the field of fluid dynamics; they proposed the smooth particle rendering (SPR) technique and applied it to visualizing astrophysical simulations of supernova explosions, interstellar cloud-cloud collisions and gas flow into a black hole.

2. Influence Function

Earthquake data are specified by hypocentral parameters, *i.e.*, location $\boldsymbol{r}_i=(x_i, y_i, z_i)$, origin time t_i, and magnitude M_i for event i. Suppose that each event has an influence at any point $(\boldsymbol{r}, t)$ in the four-dimensional space. Let us denote $P(|\boldsymbol{r}-\boldsymbol{r}_i|, M_i)$ and $T(t-t_i, M_i)$ as the space and time functions for the influence, respectively.

We assume that the influence function for all earthquake events is obtained by superposing those for individual events, as written in the form

$$f(\boldsymbol{r}, t)=\sum_{i=1}^{N} A(M_i)P(|\boldsymbol{r}-\boldsymbol{r}_i|, M_i)T(t-t_i, M_i)\,, \tag{1}$$

where $A(M)$ represents the intensity of the activity in an event of magnitude M, and N is the total number of events. One of the simple smoothed spatial functions is Gaussian, i.e.,

$$P(r, M)=\exp(-r^2/\sigma^2(M))\,, \tag{2}$$

where $\sigma(M)$ is a length scale for the influence. Another form adopted in this paper is quadratic such that

$$\begin{aligned} P(r, M)&=(1-r/\sigma(M))^2 \qquad \text{for } r\leq\sigma(M) \\ &=0 \qquad\qquad\qquad\quad r>\sigma(M)\,. \end{aligned} \tag{3}$$

The above functions are isotropic and have only one parameter for the spatial dimension, the length scale. It is possible to relate the parameter to the extent of a seismic influence, such as the range of a seismic gap created before an earthquake and the scale of an aftershock region in a broad sense. The decay of the influence is modeled to be exponential in time on the analogy of relaxation phenomena in various physical problems as follows:

$$\begin{aligned} T(t, M)&=\exp(t/\tau_1(M)) \qquad \text{for } t\leq 0 \\ &=\exp(-t/\tau_2(M)) \qquad \text{for } t>0\,, \end{aligned} \tag{4}$$

where the time constants $\tau_1(M)$ and $\tau_2(M)$ represent the precursory effect and aftereffect of the earthquake, respectively. In some actual cases, the range of the seismic gap expands before a target earthquake and diminishes after the event following the above time dependence (TSUKUDA, 1989b).

The function $f(\boldsymbol{r}, t)$ serves as a creator of the input grid data for the volume rendering procedure. Figure 2 illustrates its spatial form. In addition to the seismic data, we treat auxiliary data which include traces of coordinate axes, geographical

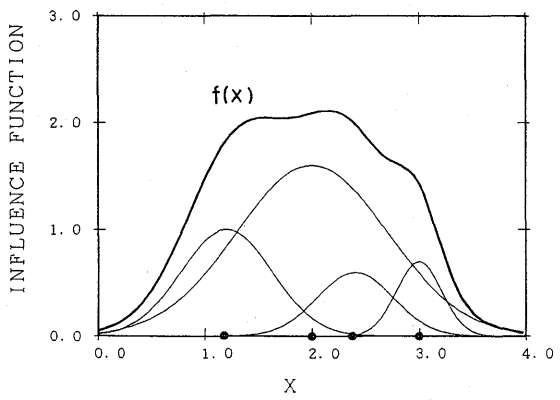

Fig. 2. Influence function for the Gaussian type spatial forms. The small solid circles represent the hypocenters.

map data and so on. All of these data are given in the form of scalar function of $\boldsymbol{r}$ similar to the influence function.

3. Volume Rendering

The configuration of the volume space and the viewing screen are shown in Fig. 3. The coordinate system (x, y, z), a transformed system from the real geographical setting, is such that the screen spans the (x, y) plane. The solid image of a 3-D body is produced on the screen by the rays arriving from the body in the direction perpendicular to the plane. Here, the hypothetical screen and the body are assumed to be kept at such a long distance that the rays are parallel. To illuminate the body, we assign a distant light source emitting parallel rays toward the body. This external light is assumed to be propagated through the medium without loss of energy by absorption, reflection or scattering.

The intensity of the ray from a volume element (voxel) along the z axis is described by the following radiation transport equation:

$$dc(x, y, z)/dz = -\beta(x, y, z)c(x, y, z) + \gamma(x, y, z)\,, \tag{5}$$

where $c(x, y, z)$ denotes the intensity of light with a specified frequency or color; $\beta(\boldsymbol{r})$ and $\gamma(\boldsymbol{r})$ are related to the absorption and radiation effects in the medium, respectively. It is convenient to rewrite $\gamma(\boldsymbol{r})$ as

$$\gamma(x, y, z) = \beta(x, y, z)s(x, y, z)\,. \tag{6}$$

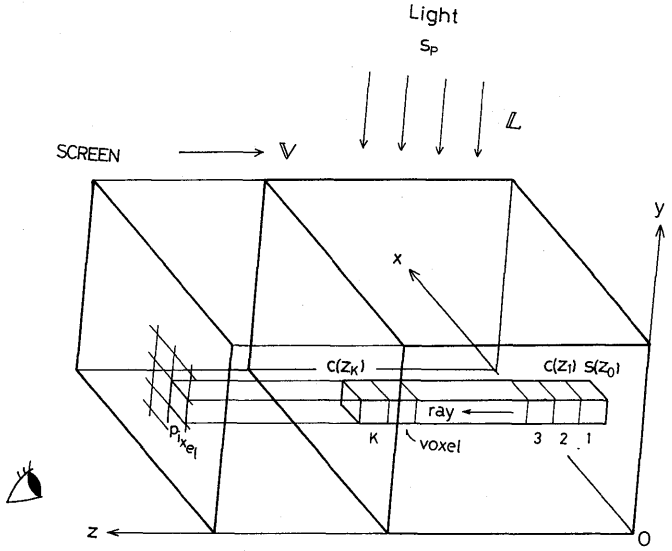

Fig. 3. Voxels, pixels and rays for sampling of volume data.
We look at the volume picture projected on the screen. The radiation transport equation (5) is applied to the voxels along z axis. For symbols and notations, see the text.

A finite difference scheme of the differential equation (5) takes the form

$$c(x, y, z_i)=(1-\alpha(x, y, z_{i-1}))c(x, y, z_{i-1})+\alpha(x, y, z_{i-1})s(x, y, z_{i-1}), \quad (7)$$

where $\alpha(x, y, z)=\Delta z\cdot\beta(x, y, z)$ and $\Delta z=z_i-z_{i-1}=\text{const.}$ $\alpha(x, y, z)$ is called opacity. We assume $\alpha(x, y, z_0)=1$. Then, iteration by Eq. (7) results in the formula

$$C(x, y)\equiv c(x, y, z_{K+1})=\sum_{k=0}^{K}\left[s(x, y, z_k)\alpha(x, y, z_k)\prod_{m=k+1}^{K}(1-\alpha(x, y, z_m))\right]. \quad (8)$$

The procedure for determining the radiation $s(x, y, z)$ is called shading. The medium is illuminated by the assigned external light source. We adopt here the following simplified version of the Phong model (BUI-TUONG, 1975) for shading:

$$\left.\begin{aligned} s(\boldsymbol{r})&=s_p[k_a+k_d(\boldsymbol{N}(\boldsymbol{r})\cdot\boldsymbol{L})+k_h(\boldsymbol{N}(\boldsymbol{r})\cdot\boldsymbol{H})^n],\\ \boldsymbol{H}&=\frac{\boldsymbol{V}+\boldsymbol{L}}{|\boldsymbol{V}+\boldsymbol{L}|},\\ \boldsymbol{N}(\boldsymbol{r})&=\frac{\nabla f(\boldsymbol{r})}{|\nabla f(\boldsymbol{r})|}, \end{aligned}\right\} \quad (9)$$

where

s_p = intensity of parallel light source,
$\boldsymbol{L}$ = normalized vector in direction of light source,
$\boldsymbol{V}$ = normalized vector in direction of observer (or screen),
$\boldsymbol{H}$ = normalized vector in direction of maximum highlight,
k_a = ambient reflection coefficient,
k_d = diffuse reflection coefficient,
k_h = specular reflection coefficient,
n = exponent used to approximate highlight.

$\boldsymbol{N}(\boldsymbol{r})$ represents the unit vector normal to the local isovalue surface of the influence function.

The images of the isovalue surfaces can be drawn on the screen by assigning opacities selectively to respective voxels. This procedure is called classification. The range of the transition region for the surface is set to be variably dependent on the steepness of the gradient of the scalar function to avoid aliasing artifacts (LEVOY, 1988):

$$\alpha(\boldsymbol{r})=\alpha_v\begin{cases} 1 & \text{if } |\nabla f(\boldsymbol{r})|=0 \text{ and } f(\boldsymbol{r})=f_v,\\ \left(1-\dfrac{1}{h_v}\left|\dfrac{f_v-f(\boldsymbol{r})}{\nabla f(\boldsymbol{r})}\right|\right) & \text{if } |\nabla f(\boldsymbol{r})|>0 \text{ and for } \boldsymbol{r} \text{ such that } \alpha(\boldsymbol{r})>0,\\ 0 & \text{otherwise}. \end{cases} \quad (10)$$

The parameters for this classification are as follows:

l = number of layers,
f_v = f value for layer v,

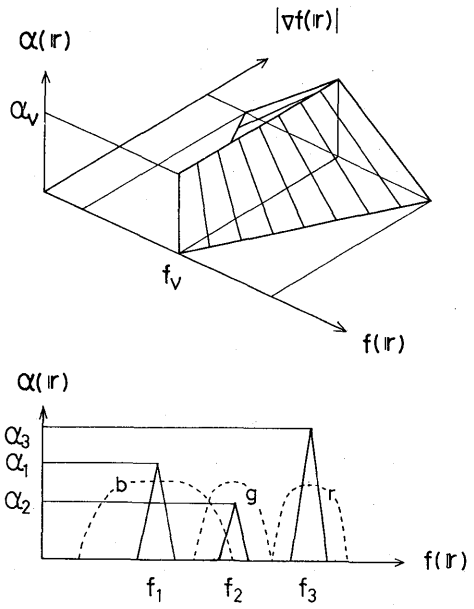

Fig. 4. Opacity determination. The upper surface is described by Eq. (10). The lower figure shows an example of a classification in which three layers are assigned; the broken lines represents the forms of the color windows defined by Eq. (11).

α_v = opacity for layer v, $0 \leq \alpha_v \leq 1$,

h_v = relative thickness of the layer,

where v is an integer and $1 \leq v \leq l$. The above opacity function is described in Fig. 4. The local gradient vector $\boldsymbol{N}(\boldsymbol{r})$, or a surface normal, is obtained analytically for the influence function (1) in terms of the spatial function (2) or (3).

The radiation $s(\boldsymbol{r})$ and opacity $\alpha(\boldsymbol{r})$ are defined separately for each color: $s_\lambda(\boldsymbol{r})$ and $\alpha_\lambda(\boldsymbol{r})$ for color λ. In this paper, the color properties are incorporated by applying the color window $w_\lambda(\boldsymbol{r})$ to the opacity function whereas $s_\lambda(\boldsymbol{r})$ is assumed to be independent of color as follows.

$$\left.\begin{aligned} s_\lambda(\boldsymbol{r}) &= s(\boldsymbol{r}) , \\ \alpha_\lambda(\boldsymbol{r}) &= \alpha(\boldsymbol{r}) w_\lambda(\boldsymbol{r}) , \\ w_\lambda(\boldsymbol{r}) &= 1 - ((f(\boldsymbol{r}) - f_\lambda)/h_\lambda)^4 , \end{aligned}\right\} \tag{11}$$

where f_λ and h_λ are the central value and width for color λ, respectively. The two processes, shading and classification, are conducted independently or in parallel. The final step is to calculate the pixel (picture cell) color data $C(x, y)$ following Eq. (8). All the pixel information is derived from the corresponding z column of voxels (Fig. 3). The procedures described above are summarized in Fig. 5.

4. Graphic Processing

A block diagram of the graphic system and devices used in this study is given in Fig. 6. The network video server iCFD NVS-2000 serves as an interface between a computer and various video instruments, i.e., a video monitor, video

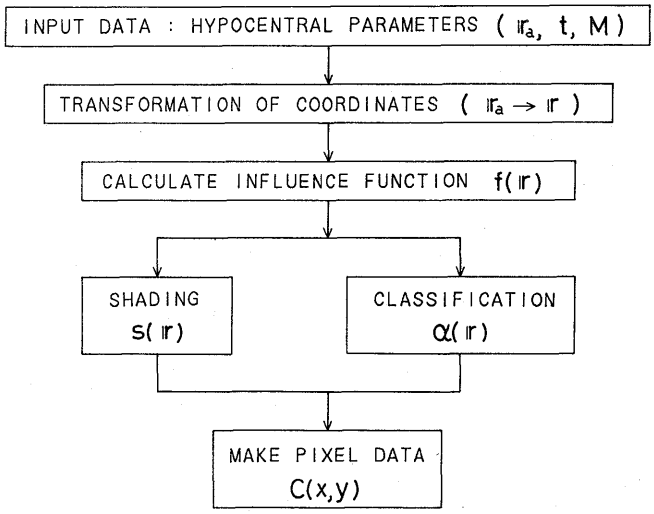

Fig. 5. Computation procedures for pixel data.

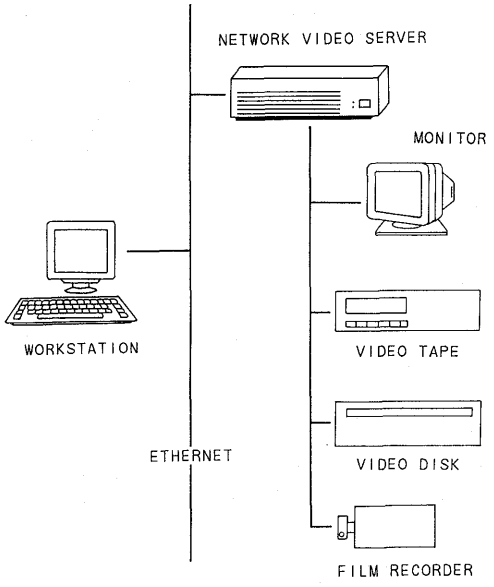

Fig. 6. Block diagram of the graphic system.

tape recorder/player units, video disk recorder/player units (SONY LVR-5000A/LVS-5000A), and a film recorder (Nippon Avionics CIR-320) with a camera. The computer and the network video server are connected via Ethernet.[1]*

The main computer we used is the high performance workstation, IBM Power Station (RISC SYSTEM/6000-550) (60 Mega Bytes). The volume space is divided

*1 Ethernet is a trade mark of Xerox Corporation.

into 320, 240 and 320 sections to define voxels for the x, y and z directions, respectively (see Fig. 3). The computation procedures do not require memorization of all the voxel data in the CPU memory. The pixel data is the final product and should be memorized to the end. The color information for each pixel contains three fundamental components, *Red*, *Green* and *Blue* (RGB). The word length for a color component is 1Byte; the total capacity of the RGB pixel data amounts to about 230 Kilo Bytes. In order to reduce computing time, weak contributions of the spatial and temporal factors in Eq. (1) are truncated. After obtaining the above color pixel data, we can expand them to more minute pixels for fine graphic pictures by interpolating the former grid data. The scale of the real graphic pixel is contracted to 1 : 2 in linear dimension in this study. The time spent to produce one picture ranges from 30 to 180 s, roughly on average 1 min, depending on the quantity of data. The computer program codes are written in C and/or FORTRAN.

The pixel data are sent to NVS-2000 via the Ethernet line. The ftp*[2] command in the UNIX*[3] operating system is used to do this. Before transfer, data are compressed to save the computer storage and to reduce the network transmission load. The RGB data is converted into standard video signals, such as analog RGB, s-video and NTSC,*[4] which can be displayed on the video monitor and stored on the video tapes and/or laser disks. The optical disk of the LVR-5000A is capable of storing about 87,000 frames of video data. A set of pictures for successive time slices provides us with movies: 30 frames per second are needed for the video monitor.

5. Application to Microseismic Data

Figures 7, 8, 9 and 10 are examples of the seismological pictures obtained by the method proposed in this paper. The object is a descending lithospheric plate within the earth, where seismic activity is very high, whereas the surrounding athenosphere has almost no seismicity. Particularly, the bent part of the plate has many microearthquakes as found in the northwestern end of the Philippine Sea Plate. Earthquake data are from the Shiraki Microearthquake Observatory, Earthquake Research Institute, University of Tokyo, of which satellite stations cover the Bungo Channel region between Kyushu and Shikoku Islands. These stations have been operated since July 21, 1983. The detailed discussions on the nature of the data and hypocentral distributions are presented by MIURA *et al.* (1991). We restrict ourselves to events with depths of 35 km or more. The total number of events is 4658. The majority (70%) have magnitudes of 2 and above. A conventional presentation of the 3-D distribution of the foci is shown in Fig. 1.

For simplicity, the external light source is specified to be located high up in the y direction for the volume rendering coordinate system. Various parameters for the functions for seismic influence, shading and classification are listed in Table

*[2] The ftp command is the interface to the File Transfer Protocol (FTP).
*[3] UNIX is a trade mark of AT & T.
*[4] NTSC: National Television Standards Committee, U.S.A.

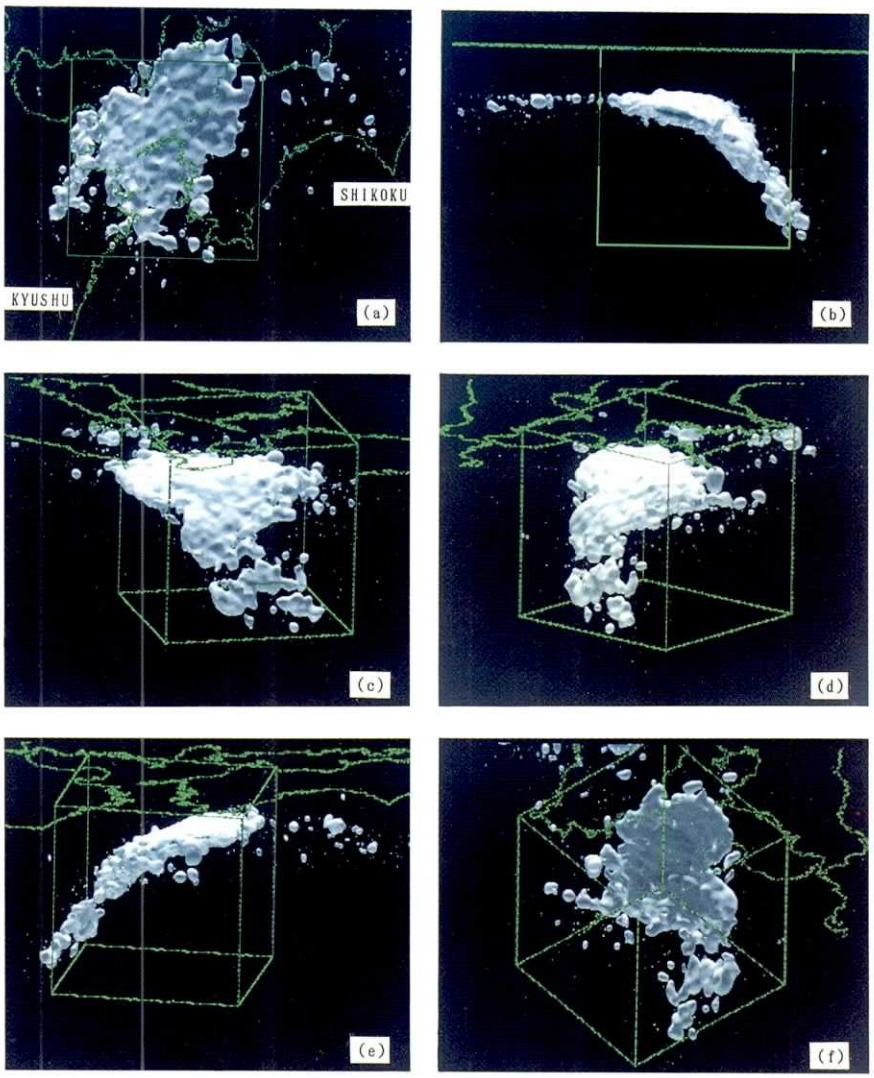

Fig. 7. Monochromatic visualization of the extent of the earthquake distribution: An inverted-triangle-shaped solid at the bending part of the subducting Philippine Sea plate with separated fragment at the deepest level up to a depth of 150 km.
The observation period is the same as that of Fig. 1. The cubic box, 150 km on each side, indicates the scale and orientation of the coordinate system. The specifications of volume rendering are listed in Table 1. (a) Top view; (b)–(e) Side views from different angles; (f) Picture viewed from beneath the ground.

1. The parameters for the description of the coastlines in geography and the box indicating spatial scales are omitted in the list. The size of the final pixel is 0.52×0.52 km except for Fig. 10, where it measures 2.08×1.04 km for x and y axes, respectively. Each figure has its own purpose as will be mentioned below.

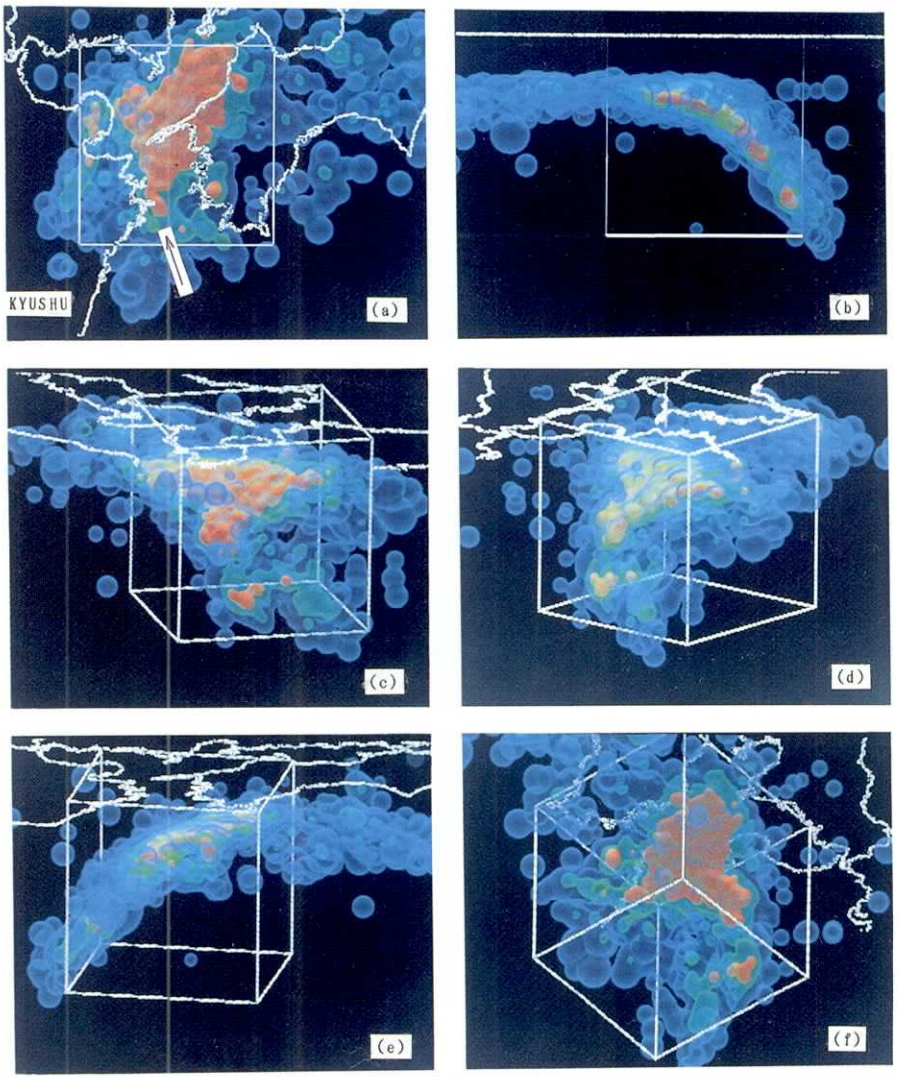

Fig. 8. Three color isovalue surfaces for activity distributions.
The data source is the same as that for Fig. 7. Figures (a)–(f) correspond to those of Fig. 7, respectively. The strong core of seismic influence is represented by red; the medium strength range by green; the weak range by blue. The details of the rendering parameters are given in Table 1. The arrow in (a) indicates the lineament, the boundary between the high and low seismic regions.

The detailed analyses and the geophysical and geological interpretations for the graphic pictures will be presented elsewhere.

5.1. 3-D shape of hypocentral distribution

Figure 7 shows monochromatic views of the outline of the continuum for

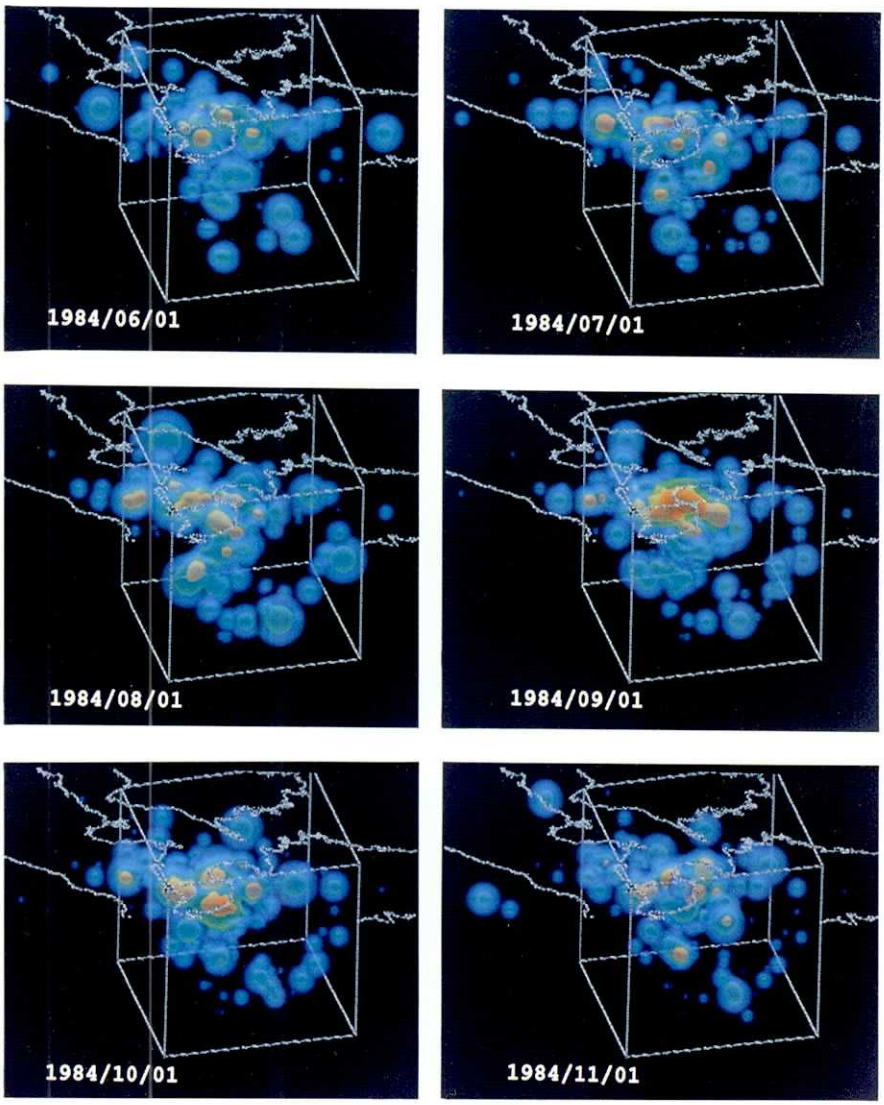

Fig. 9. Temporal change of the activity for a fixed viewing angle.

the densely distributed hypocenters. We only pay attention to the locations of foci and density of the points without considering magnitudes. We adopted the quadratic type rather than the Gaussian type for the spatial function. The reason is that the effective spatial coverage of the influence function should be as small as possible while the foot of the lobe should be long enough to keep continuity in the sum of the influence functions with respect to neighboring foci.

The curved upper surface of the inverted-triangle-shaped seismic region described in Fig. 7 should delineate the uppermost part of the lithospheric plate. The vertical cross section of the surface in the direction of N75°W is almost

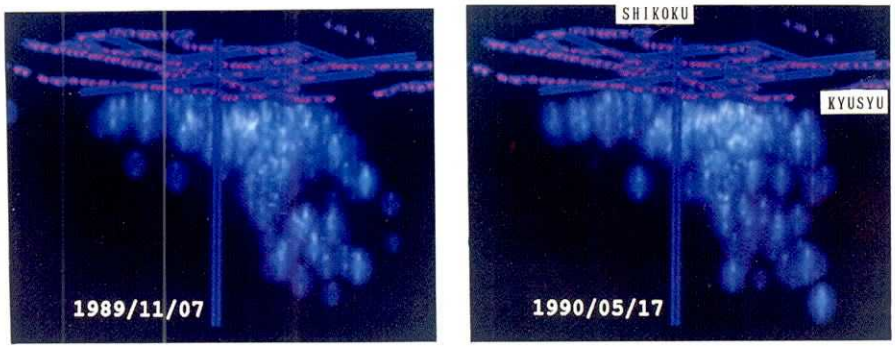

Fig. 10. Formation of the seismicity gap.
The vertical scale is two times as large as the horizontal one. A remarkable seismic event took place at the center of the gap (right).

Table 1. Parameters for each figure. M denotes magnitude. The colors, red, green and blue, are abbreviated as r, g, b, respectively. See the text for other notations.

Item	Fig. 7	Fig. 8	Fig. 9	Fig. 10
Intensity Function				
$A(M)$	$=1$	$=M$	$=M$	$=M$
Spatial Function	Eq. (3)	Eq. (2)	Eq. (2)	Eq. (2)
$\sigma(M)$	8.0 km	$1.6M$ km	$2.4M$ km	$6.0M$ km
Time Function	$=1$	$=1$	Eq. (4)	Eq. (4)
$\tau_1(M)$			20 days	20 days
$\tau_2(M)$			80 days	80 days
Shading				
k_a	0.2	0.5	0.5	0.8
k_d	0.8	0.5	0.5	0.5
k_h				1.0
n				20
Classification				
v (layer number)	1	1 2 3	1 2 3	1 2
f_v	1.0	0.2, 5.0, 20.0	0.02, 2.0, 8.0	0.04, 2.0
α_v	0.5	0.2, 0.2, 1.0	0.05, 0.1, 1.0	0.08, 0.2
h_v	2.0	1.0, 1.0, 2.0	8.0, 3.0, 4.0	0.08, 0.2
Color Window				
λ (color index)		b g r	b g r	b g
f_λ	1.0	0.0, 5.0, 20.0	0.0, 1.4, 6.0	0.0, 20.0
h_λ	10.0	4.0, 5.4, 10.0	1.4, 1.4, 5.6	20.0, 20.0

circular arc with a radius of curvature of 121 km, suggesting the existence of a bending force exerted on the plate in addition to the negative buoyancy due to self-gravitation (TSUKUDA and MIURA, 1991). The thickness of the seismic layer is within 20 km (MIURA *et al.*, 1991).

5.2. *Activity structure in the seismic zone*

Figure 8 describes the intensity of the seismicity and its internal structure. Three surface layers are classified by the parameters as listed in Table 1. The designated colors are blue, green and red according to the intensity of the influence function.

The most striking feature is the clear cutoff of the high activity region forming a lineament image at the southern and northern sides of the inverted triangle. Parallel stripes to these are also recognized in the zone of the triangle. The red core seen in the side views of the slab earthquake zone discloses the existence of a thin seismic plane.

5.3. *Temporal variation of the activity structure*

Figure 9 is a modified version of Fig. 8, incorporating time dependence. The uppermost region of high curvature for the descending plate frequently has a considerable amount of seismic activity. The figure represents one of those periods; the peak occurred around September, 1984. Synchronized activity forms a broad red core. The lineaments of red or green images seen in the respective time steps are also evidence of the synchronization of activity.

5.4. *Blurred distribution of earthquakes and its temporal change*

If we choose suitable parameters of the shading, classification and color specification, a blurred image of seismicity such as Fig. 10 is obtained. This version is appropiate for recognizing a seismic gap and so-called doughnut activities surrounding the gap. As MOGI (1979) proposed, the center of the doughnut would be a possible site of a future strong earthquake.

6. Concluding Remarks

This paper is the first report on the application of a volume rendering technique to the study of seismicity, and the main purpose is to make clear the methology. Therefore, the forms of the influence functions and the values of rendering parameters were not extensively discussed here. Making physical sense of the parameters is left for future studies.

The semi-transparent volume rendering method has proved to be greatly efficient for us to detect synchronized activities, linear configurations of earthquakes during a certain period, and the creation processes of seismic gaps with surrounding activity known as "doughnut" phenomena. Finding of these phenomena would contribute to the study of earthquake prediction. The use of this method can be extended to analyzing other seismological and geophysical data provided that the volume data are given by scalar functions with respective to space position.

References

BUI-TUONG,P., 1975, *CACM*, June 1975, 311–317.

KELLER, J. A., 1970, Space-time seismicity of the Alaska-Aleutian seismic zone, *J. Geophys. Res.*, **75**, 5745–5756.

LEVOY, M., 1988, Display of surfaces from volume data, *IEEE Computer Graphics and Applications*, **8**, 29–37.

MIURA, K., T. TSUKUDA, R. MIURA, Y. INOUE and S. ASANO, 1991, Deep seismic zone in the western part of the Seto Naikai (Seto Inland Sea) and its surrounding regions, southwestern Japan, *Bull. Earthq. Res. Inst.*, **66**, 553–570 (in Japanese).

MIZOUE, M., M. NAKAMURA and K. KOTANI, 1975, Characteristics of seismicity in the northwestern part of the Kii peninsula—in special reference to the active fault system as inferred from spatial distributions of small and micro-earthquakes—, *Pub. 50th Ann. Great Kanto Earthq., Earthq. Res. Inst.*, 199–216 (in Japanese).

MOGI, K., 1968, Migration of seismic activity, *Bull. Earthq. Res. Inst.*, **46**, 53–74.

MOGI, K., 1979, Two kinds of seismic gaps, *Pure Appl. Geophys.*, **117**, 1172–1186.

NAGASAWA, M. and K. KUWAHARA, 1991, Smoothed particle rendering for fluid visualization in astrophysics, in *Scientific Visualization of Physical Phenomena* (ed. N. M. Patrikalakis, Springer-Verlag, Tokyo), 589–605.

OIKE, K., 1976, Spatial and temporal distribution of micro-earthquakes and active faults, *Mem. Geol. Soc. Japan*, No. 12, 59–73 (in Japanese).

OIKE, K., 1980, On the activity of microearthquakes in the Yamasaki fault region, *Proc. Earthquake Predict. Res. Symp.*, 1980, 155–158 (in Japanese).

PATRIKALAKIS, N. M. (ed.), 1991, *Scientific Visualization of Physical Phenomena*, Springer-Verlag, 690 pp.

THALMANN, D. (ed.), 1990, *Scientific Visualization and Graphics Simulation*, John Wiley & Sons, 264 pp.

TSUKUDA, T., 1989a, Seismicity map depending on the laspe times and magnitudes of earthquakes, *PROGRAMME and ABSTRACTS, Seism. Soc. Japan*, 1989 No. 1, 144 (in Japanese).

TSUKUDA, T., 1989b, Expansion and contraction of seismicity gap associated with remarkable earthquakes, *PROGRAMME and ABSTRACT, Seism. Soc. Japan*, 1989, No. 2, 141 (in Japanese).

TSUKUDA, T., 1990, Some characteristics of the seismicity in the northern Fossa Magna, central Japan, *J. Geography*, **99**, 32–42 (in Japanese).

TSUKUDA, T. and K. MIURA, 1991, Bending moment for subducting slab—at the northwestern end of the Philippine Sea Plate—*PROGRAMME and ABSTRACTS, Seism. Soc. Japan*, 1991 No. 2, 320 (in Japanese).

地震活動のボリューム・ビジュアライゼーション

佃　為成[1)]・三浦勝美[1)]・藤原公昭[2)]
英　憲悦[3)]・山下輝夫[1)]

1) 東京大学地震研究所
2) (株) 計算流体力学研究所
3) (株) SIG

地震活動の時空間分布を semi-transparant volume rendering 法を用いてコンピュータグラフィックスで表現する新しい方法を開発した．震源距離やマグニチュードに依存した各地震の影響を足し合わせ，空間の各地点における影響関数（スカラー）を定義した．この影響関数が 3 次元空間の媒質とその時間変化を規定する．この物体に外部から光を当てると，Shading パラメータに従った反射や散乱の結果，物体が発光して見える．媒質には不透明度が付与されるが，影響関数の

値に対して選択的に定義すると等値面を作り出すことができる (Classification). Shading や classification では光の色についても指定できる．この方法を用いて伊予灘・豊後水道直下のやや深発地震の活動のビジュアライゼーションを試みた．震源の3次元分布の形状の把握や活動線の確認，空白域の形成過程の観察などに有効であることが確かめられた．この方法はほかの地球物理データやシミュレーション結果の表示にも応用できる．